

Active faulting and continental slope instability in the Gulf of Patti (NE Sicily, Italy): a field, marine and seismological joint analysis

Cultrera F.*¹, Barreca G.¹, Burrato P.², Ferranti L.³, Monaco C.¹, Passaro S.⁵, Pepe F.⁶
& Scarfi L.⁷

Corresponding email: fcultrera@unict.it

1. Dipartimento di Scienze Biologiche, Geologiche e Ambientali - Sezione di Scienze della Terra, Università di Catania.
2. Istituto Nazionale di Geofisica e Vulcanologia, Roma 1.
3. Dipartimento di Scienze della Terra, delle Risorse e dell'Ambiente, Università di Napoli "Federico II".
4. Dipartimento di Matematica e Geoscienze, Università di Trieste.
5. Istituto per l'Ambiente Marino Costiero, C.N.R. Napoli.
6. Dipartimento di Scienze della Terra e del Mare, Università di Palermo.
7. Istituto Nazionale di Geofisica e Vulcanologia, Osservatorio etneo, Catania

Abstract

The Gulf of Patti and its onshore sector represents one of the most seismically active region of the Italian Peninsula. Over the period 1984–2014, about 1800 earthquakes with small-to-moderate magnitude and a maximum hypocentral depth of 40 km occurred in this area. Historical catalogues reveal that the same area was affected by several strong earthquakes such as the Mw=6.1 event in April 1978 and the Mw=6.2 one in March 1786 which have caused severe damages in the surrounding localities. The main seismo-tectonic feature affecting this area is represented by a NNW–SSE trending right-lateral strike-slip fault system called “Aeolian-Tindari-Letojanni” (ATLFS) which has been interpreted as a lithospheric transfer zone extending from the Aeolian Islands to the Ionian coast of Sicily. Although the large-scale role of the ATLFS is widely accepted, several issues about its structural architecture (i.e., distribution, attitude, and slip of fault segments) and the active deformation pattern are poorly constrained, particularly in the offshore. An integrated analysis of field structural geology with marine geophysical and seismological data, has allowed to better understand the structural fabric of the ATLFS which, in the study area, is expressed by two major NW-SE trending, en-echelon arranged fault segments. Minor NNE-SSW oriented extensional structures mainly occur in the overlap region between major faults, forming a dilatational stepover. Most faults display evidence of active deformation and appear to control the main morpho-bathymetric features. This aspect, together with diffused continental slope instability, must be considered for the reevaluation of the seismic and geomorphological hazard of this sector of southern Tyrrhenian Sea.

1. Introduction

The Gulf of Patti, in the Tyrrhenian side of NE Sicily (southern Italy, Fig. 1A), is a densely populated area that hosts several villages, a number of strategic industrial sites and seabed infrastructures (e.g. electric power and telecommunications cables). As documented by seismological data, this area has been struck in historical times by a number of $M \sim 6$ earthquakes which caused severe damages in the whole coastal area and surrounding region (Gasparini et al.,

49 1982, 1985; Rovida et al., 2011). A high-rate seismicity (more than 2000 events in the last 30 years)
50 is currently registered in the Gulf of Patti and the distribution of events forms a roughly NNW-SSE
51 trending seismic belt (Fig. 1B). The latter has been interpreted as related to the activity of a major
52 fault system running across NE Sicily and known as the Aeolian–Tindari–Letojanni Fault System
53 (ATLFS in Fig. 1C, see Ghisetti, 1979; Locardi and Nappi, 1979; Lanzafame and Bousquet, 1997,
54 Palano et al., 2012). This fault system is a major tectonic boundary separating the western Calabria-
55 Peloritani extensional belt, to the east, from the north Sicily continental collision zone to the west
56 (see inset in Fig. 1C) (e.g. Lanzafame and Bousquet, 1997, Nicolich et al., 2000; Doglioni et al.,
57 2001; Faccenna et al., 2004; Chiarabba et al., 2008, Goes et al., 2004; Neri et al., 2004; Pepe et al.,
58 2000; Pepe et al., 2005; Billi et al., 2006; Palano et al., 2012; Barreca et al., 2014). Notwithstanding
59 its geodynamic role, the northern part of the ATLFS, which runs across the Gulf of Patti, poses a
60 significant seismic hazard in the region. Furthermore, new high resolution swath bathymetry and
61 seismic data, just to the east of the investigated area (Rovere et al., 2014), revealed an highly
62 unstable continental slope with the occurrence of large submarine slides, capable of mobilizing
63 huge volumes of material. The overall regional instability is increased by the over-steepening
64 caused by the high rate (1-2 mm/yr) uplift that affects the coastal areas, as confirmed by raised
65 Pleistocene and Holocene paleo-shorelines (Ferranti et al., 2006; Scicchitano et al., 2011). The
66 coupling of intense seismo-tectonic deformation and critical morpho-dynamic conditions in the
67 offshore makes the studied region one of the most critical area of southern Italy in terms of geo-
68 hazard.

69 In this paper we present the results of integrated onshore/offshore analyses focused on the
70 characterization of active faults and stability of submarine slopes. The study is based on
71 seismological, field structural and marine geophysical data (seismic reflection and swath
72 bathymetry), to provide a comprehensive assessment of the potential hazards affecting the area.

73

74 **2. Tectonic framework**

75 *2.1. General outlines*

76 North-eastern Sicily is a crucial tectonic domain within the central Mediterranean orogeny
77 (Fig. 1A), which ensues from the Neogene-Quaternary convergence between the European and
78 African plates (Barberi et al., 1974; Patacca et al., 1990; Faccenna et al., 2001). The ~N-S trending
79 tectonic shortening has progressively involved a laterally variable pre-orogenic domain,
80 characterized by the Hyblean continental block (HB in Fig. 1A) and the adjacent Ionian oceanic
81 lithosphere on the African side, which subducted beneath Europe. In north-eastern Sicily the
82 resulting contractional belt is formed by two major superposed structural levels, the Calabro-

83 Peloritani terrane and the underlying Sicilian fold and thrust belt, deriving from the detachment and
84 overthrusting of portions of the North African paleomargin.

85 The Calabro-Peloritani terrane (CPT in Fig. 1C) is largely exposed in north-eastern Sicily
86 where it forms the backbone of the Peloritani mountains. The thrust stack consists of imbricate
87 sheets of Hercynian metamorphic rocks and associated Meso-Cenozoic sedimentary covers
88 (Ogniben, 1969). The Africa-derived units occupy the central and western portion of Sicily (SFTB
89 in Fig. 1C) and involves thrust sheets represented by Meso–Cenozoic shallow marine to open shelf
90 sedimentary rocks. During the convergence, the subduction and rollback of the Ionian oceanic
91 lithosphere (Barberi et al., 1974; Malinverno and Ryan, 1986; Scarascia et al., 1994; Gueguen et al.,
92 1998; Gvirtzman and Nur, 1999; Doglioni et al., 2001; Faccenna et al., 2001, 2004) favored
93 lithospheric thinning and formation of the Tyrrhenian Basin in the back-arc region (Fig. 1A).

94 The articulated morphology of the North African paleomargin strongly influenced the
95 migration pattern and rate of the upper plate of the subduction system (Faccenna et al., 2004).
96 Indeed, while the orogenic belt migrated at a rate of 1–2 cm/yr during the last 5–6 Myr in northern
97 Sicily and in the Southern Apennines (Ferranti and Oldow, 2005), north-eastern Sicily and Calabria
98 experienced a more rapid (5–6 cm/yr) E to SE motion (Goes et al., 2004). The relatively lower rate
99 of migration of the orogenic belt is explained by the involvement in the collision zone of the
100 Pelagian and Apulian continental blocks alongside the subducting and retreating Ionian oceanic slab
101 beneath northeastern Sicily and Calabria. The different rates of motion above the continental vs.
102 oceanic segments of the African-Adriatic margin caused the curved shape of the accretionary
103 wedge, lithospheric wrenching at slab edges (Wortel and Spakman, 2000; Govers and Wortel,
104 2005; Gutscher et al., 2015; Barreca et al., 2016; Polonia et al., 2016) and strong back-arc extension
105 in the central part of the Tyrrhenian basin (Gueguen et al., 1998; Faccenna et al., 2004; Rosenbaum
106 and Lister, 2004).

107

108 *2.2. Current kinematics and Seismotectonics*

109

110 The current kinematics of north-eastern Sicily and southern Calabria is dominated by the
111 subduction and roll-back of the Ionian slab (Faccenna et al., 2001). A $\sim 70^\circ$ Benioff-Wadati zone
112 dipping towards the NW, beneath the southern portion of the Tyrrhenian Basin, has been
113 documented since the early 1970s (Chiarabba et al., 2005 and reference therein) by sub-crustal
114 earthquakes occurring down to a depth of 600 km (Frepoli et al., 1996) and by a body of high-
115 velocity anomaly within the upper mantle (Selvaggi and Chiarabba, 1995; Faccenna et al., 2004;
116 Neri et al., 2012). The different rate of motion between north-eastern Sicily and Calabria and the

117 adjacent colliding domains results in wrenching at the edges of the migrating upper plate block and
118 tearing at depth (Govers and Wortel., 2005; Gutscher et al., 2015; Barreca et al., 2016; Polonia et
119 al., 2016), where the slab is thought to detach from adjacent continental sectors, a process known as
120 “Subduction Transfer Edge Propagator” (STEP) faulting (Govers and Wortel., 2005). Govers and
121 Wortel (2005) have proposed the ATLFS as the surface expression of such STEP fault zone (see
122 also Gallais et al., 2013).

123 The northern part of the ATLFS consists of a swarm of NNW–SSE trending transtensional
124 faults which extends from the Aeolian Islands to the Tyrrhenian coast of Sicily between Capo
125 Milazzo and Capo Tindari. Dextral transtension along this belt is confirmed by GPS estimation of
126 ~3.6 mm/yr of extension along the N126E direction (Palano et al., 2012). This regional
127 discontinuity is regarded to have a primary role in the seismo-tectonics of this sector since it is
128 currently marked by intense seismicity and it is spatially related to strong historical earthquakes
129 (Fig. 1C). A major historical event associated with the activity of the ATLFS occurred on March
130 10, 1786 (MCS maximum intensity of IX with an estimated magnitude of 6.2, see e.g.,
131 <http://emidius.mi.ingv.it/CPTI> by Rovida et al. 2011) causing the destruction of several villages
132 facing the Gulf of Patti. In addition, a Mw= 6.1 earthquake occurred in the Gulf of Patti on April
133 15, 1978, about 10 km west of Capo Milazzo (Gasparini et al., 1982, 1985, Rovida et al. 2011). The
134 earthquake hit primarily the Tyrrhenian side of northeastern Sicily but was also felt over a large part
135 of Sicily and Calabria. Significant damages and collapses occurred in about 100 sites along the Gulf
136 of Patti coast and also in the Aeolian Islands (Barbano et al., 1979). More recently (in August
137 2010), the area was affected by significant seismic energy released by a M=4.8 event located 9 km
138 SW of the Vulcano island. The seismic event was widely felt in northeastern Sicily and caused
139 some damage on a number of masonry buildings (see Azzaro et al., 2014).

140

141 3. Field data

142 A detailed morpho-structural analysis has been performed in the on-land sector, where
143 meso-faults and fractures attitudes were collected at 40 key sites (see crossed hammers in Fig. 2A
144 and cumulative plots). Slip vectors on fault planes were obtained when steps, or more rarely,
145 slickensides and Riedel fractures, were present.

146 The Gulf of Patti is a fault-controlled morphological depression (Billi et al., 2006), also
147 extending on-land (Fig. 2A), and it is filled by Plio-Quaternary marine to continental deposits (Di
148 Stefano and Lentini, 1995). Structural measurements highlight that tectonic deformation of the area
149 is expressed by two main fault populations characterized by different trends and kinematics. As
150 already evidenced by previous studies (e.g. Billi et al., 2006 among many others), the main set is

151 represented by a NW-SE to NNW-SSE trending oblique (transtensional) faults system which
152 develops from Capo Tindari to the village of Novara (Fig. 2A). Faults related to this system are well
153 exposed along the ~200 m high cliff of the Tindari promontory (Fig. 2B). N150-160E trending, 65-
154 80° dipping fault surfaces sometime exhibit a double generation of slickenlines, the younger of
155 which plunging at ~ 60° towards N130E (Fig. 2C). To the south, between Belvedere and Novara
156 villages, the fault array is oriented ~N150E and fault planes dip towards the NE at about 70°.
157 Kinematic indicators on mesofaults associated to a well-developed cataclastic zone suggest
158 extensional and strike-slip sense of motion (see stereoplot 1 in Fig. 2A).

159 A second faults system, NNE-SSW oriented, is developed on the eastern part of the on-land
160 basin where it displaces middle Pleistocene deposits (Fig. 2D). It is mainly composed of steeply-
161 dipping (70-80°), N5-25E oriented faults with pure (~90° pitch) normal sense of motion (Fig. 2E
162 and stereoplot 2 in Fig. 2A).

163 As a whole, measured faults pattern depicts a triangular-shaped deformation zone with a
164 major NNW-SSE trending bounding transtensional fault system (the Tindari-Novara segment) to
165 the west, and a secondary NNE-SSW extensional faults array to the east. Our data are in good
166 agreement with previous works in the area (Billi et al.,2006; De Guidi et al., 2013).

167 The recent and current activity of the described faults systems is not precisely constrained
168 on-land because of the lack of Holocene sediments. However, several morphological clues, such us
169 straight fault scarps and fresh triangular facets (see De Guidi et al., 2013), suggest a recent activity
170 for both fault systems.

171

172 **4. Offshore data**

173 In order to map the offshore prosecution of the two fault systems detected on-land and to
174 constrain their possible recent activity, we used a grid of very-high-resolution (sub-bottom chirp)
175 and (Sparker) single-channel reflection seismic data acquired in the continental shelf and in the
176 upper slope of the Gulf of Patti, coupled with swath bathymetry. The lines run mainly in the NE-
177 SW direction and are tied by lines acquired in NW-SE direction (see Fig. A1 for location). On the
178 whole, the reflection seismics provide an integrated image at different resolution/penetration of the
179 uppermost Quaternary succession in the Gulf of Patti and farther to the north. A brief description of
180 equipment used for data acquisition as well as detail on data processing is reported in Appendix.

181 *4.1 Swath bathymetry*

182 Bathymetric data were acquired using an EM710 Simrad (Kongsberg©inc) echo-sounder,
183 which emits more than 400 beams included in a 140° swath coverage for each ping. This equipment

184 allow to collect soundings until 2800 m below the sea-floor (bsf). All pings were processed by hand
185 to remove data outliers using Fledermaus 3D software. The processed depth measurements were
186 then organized in 20X20 m regularly spaced matrix called Digital Terrain Model (DTM, Fig. 3A).
187 The final DTM covers about 1100 km² of seafloor surface in the -1276/-22 m b.s.l. elevation range
188 and include a partial view of the Patti and Milazzo shelves, the slope area comprised between the
189 northern Sicily coast and a partial view of the distal, SE sector of the Vulcano island.

190 Seafloor morphology data revealed the occurrence of a poorly-developed continental shelf
191 which extends discontinuously from north of Capo Tindari to the westernmost sector of Capo
192 Milazzo, where it appears almost completely obliterated by retrogressive erosion sparked by the
193 presence of two canyon branches, that we named Colantoni, the easternmost, and Fanucci, the
194 westernmost (Paolo Colantoni and Francesco Fanucci were emeritus professors of marine geology
195 for several Italian universities and research centers. They passed away in 2015 and 2014,
196 respectively). The overall shape of the continental shelf reflects the general trend of the coastline in
197 map view. In detail, it dips to the north and exhibits a marked shelf break with a step of about 5 m
198 along the -150 m isobaths. The most relevant morpho-bathymetric features in this sector are the
199 large submarine canyons, that have deeply incised the continental slope. The most prominent
200 undersea relief is the Patti Ridge (Fig. 3A) which extends for about 15 km from the Tyrrhenian
201 coastline, in the SE, to the southern flank of the Vulcano island, in the NW. Particularly, the ridge is
202 represented by an asymmetric culmination which rises up to -450 m b.s.l. and it is characterized by
203 a gently sloping SW flank, incised by the Patti Valley, and a steeper NE slope (see bathymetric
204 profile A-A' in Fig. 3A) which in turn represents the SW flank of the adjacent Milazzo Canyon.
205 This last is the most impressive submarine incision occurring in the eastern part of the investigated
206 sector (see Fig. 3A), just to the east of the Patti Ridge. It is expressed by a NW-SE trending ~15 km
207 long and more than 300 m deep (see bathymetric profile B-B' in Fig. 3A) submarine incision. The
208 canyon has a sinuous path and a flat thalweg that upstream bifurcates in two minor incisions, i.e.
209 Colantoni and Fanucci branches (see above). The headwalls of the upstream incisions roughly
210 corresponds to the coastline, thus testifying the active retrogressive erosion in the area.

211 The high-resolution multibeam data allowed for the mapping of several submarine slides
212 (white polygons and/or yellow jagged lines in Fig. 3A) that are mainly distributed along the steepest
213 flanks of the major canyons. These zones of slope instability were identified by morphological
214 inspection of DTM, thanks to some peculiar tracts (depressed sectors that often exhibit a wide
215 spectrum of seabed morphologies spanning from undulated to heavily rugged). These
216 morphological characters are typical of sediment gravity flow processes (e.g., debris flows).
217 However, evidence of deep-seated gravitational slope deformation has been found ca. 5 km off the

218 coastline along the western flank of the Fanucci branch. Here, gravitational deformation is
219 expressed by a wide ($\sim 5.5 \text{ km}^2$) collapsed area that underlies to a $\sim 75\text{-m}$ -high amphitheater-shaped
220 headwall (Fig. 3B). As also suggested by sub-seafloor data (see next section 4.2), this structure may
221 be interpreted as the seafloor expression of a large slip surface involving the western flank of the
222 Fanucci branch.

223

224 *4.2 Seismic reflections profiles*

225 *4.2.1 Seismic stratigraphy*

226 A number of depositional sequences bounded by unconformities or correlative para-
227 conformities were recognized on Sparker profiles in the first 200-300 m below the sea-floor (bsf).
228 The most recent sequence overlays a widespread erosional surface that ostensibly formed during the
229 sea level stillstand of the Last Glacial Maximum (LGM, see Sparker profile SP 13 in Fig. 4),
230 whereas a stack of depositional sequences, which are interpreted as representing the falling and
231 low-stand systems tracts, record older Middle-Late Pleistocene eustatic cycles. In high-resolution
232 seismic profiles the most recent sequence is expressed by well-stratified, laterally continuous, high-
233 amplitude reflectors with typical thickness of 30-40 m. This stacking pattern is typically observed in
234 the central Mediterranean shelf and upper slope affected by vertical tectonic movements ([Chiocci et al., 1997](#);
235 [Ridente and Trincardi, 2002](#); [Pepe et al., 2003, 2014](#); [Kuhlamann et al., 2015](#)).

236

237 *4.2.2 Fault pattern*

238 A variety of structural discontinuities is observed across the Gulf of Patti and farther to the
239 north. Although they rarely show displacements larger than a few tens of meters, they document
240 tectonic regimes active in the region through time. Fault systems probably associated with negative
241 flower structures are observed at shots 2700–3700 (see Sparker profile SP 19 in Fig. 5A). They
242 consist of NNE-SSW to \sim N-S trending (the strike was derived by correlation with adjacent lines)
243 steeply-dipping extensional structures forming narrow (1-2 km wide) horst and graben associations
244 (Fig. 5B). Faults exhibit small displacements (3-20 m) and some of them also deform the seafloor
245 producing 15-20 m-high and straight scarps. Wipe-out zones are often observed near faults traces,
246 suggesting the presence of trapped fluids that ascend through fault zones (Fig. 5B). Some faults are
247 sealed by Upper Quaternary sediments but small-scale active faults can be clearly observed.
248 Particularly, the Chirp profile CHP 43 (Fig. 5C) shows a SW-dipping active normal (or
249 transtensional) fault that deforms the seafloor of about 3 m (zoom in Fig. 5D). The whole seismic
250 dataset and the bathymetric map suggest that this fault segment is at least 5.8 km-long and it
251 belongs to a larger NW-SE oriented fault zone developed along the Patti Valley.

252 Similar to those observed on-land, fault systems are arranged into two azimuthal domains,
253 NNE-SSW and NW-SE trending. NW-SE striking structures have been detected in the central (i.e.
254 along the Patti Valley) and NE portion (i.e. along the NE flank of the Patti Ridge) of the
255 investigated sector and mainly consist of normal (or transtensional) faults. These tectonic features
256 form a large fault zone, running from the SW of Capo Milazzo to the SE flank of the Vulcano
257 Island, which roughly follows the trend of the Milazzo canyon and of the adjacent Patti Ridge (see
258 above). The latter appears as a fault-bounded bathymetric culmination (Fig.5E). NNE-SSW
259 trending extensional faults occur only in the central sector of the Gulf of Patti where they form horst
260 and graben associations (Fig. 5B). Based on the integration of the new structural data coupled with
261 data available in literature (e.g. [Gabbianelli et al, 1996](#); [Cuppari et al., 1999](#); [Colantoni et al., 2001](#);
262 [Argnani et al., 2007](#)) a simplified structural map of the Gulf of Patti and its northern prolongation
263 (Fig. 6) is here proposed.

264 Seismic profiles also document widespread non-tectonic deformation (see section 4.1).
265 Indeed, a landslide-related slip surface can be observed in the Sparker profile SP 10, which crosses
266 the continental shelf between Capo Tindari and Capo Milazzo in SW-NE direction (Fig. 7A and
267 inset 1 for location). The slip surface has developed on the western flank of the Fanucci branch and
268 it dips toward the east, coherently with the downslope direction. The detachment at the base of the
269 submarine slide displays an average inclination of about 75° and progressively becomes horizontal
270 at depth. Upslope, it displaces the seabed and creates a ~ 75 m-high, circular-shaped scarp (see inset
271 2 in Fig. 7A and section 4.1). Elsewhere, along a NNW-SSE section across the continental slope,
272 the Sparker profile SP 13 also provides morphological evidences of concave-upward sliding
273 surfaces that involve and displace finely-laminated sediments that, on the whole, testify slope
274 instability processes (i.e. slumping, Fig. 7B, see inset for location). These features occur over a 4
275 km-long area and include a series of undulations of the seafloor, suggesting this is an ongoing
276 process.

277

278 **5. Seismological data**

279 The analysis of the seismic activity has been carried out referring to national and local
280 catalogues (see: <http://csi.rm.ingv.it/>; <http://www.ct.ingv.it/ufs/analisti/catalogolist.php>) which
281 include earthquakes hypocentral parameters. The selected events have been properly filtered to
282 consider only well located earthquakes (i.e. maximum azimuthal gap of 240° , root mean square
283 (rms) residuals < 0.3 sec and standard location errors (Erh and Erz) < 3.0 km and a maximum
284 hypocentral depth of 40 km). Over the period 1984–2014, about 1800 seismic events with $1.0 \leq ML$
285 ≤ 4.8 occurred in the area between the Vulcano island and the mainland of the Gulf of Patti (Fig.

286 8A). In general, the map distribution of events depicts a ~ 10-15 Km wide and NW-SE trending
287 seismic belt that, at a more detailed scale, is composed of several NE-SW oriented clusters which
288 can be observed in the offshore just west of Capo Milazzo. On-land, where many earthquakes
289 occurred as swarms (see Scarfi et al., 2005; Giammanco et al., 2008), preferential events
290 distribution is more difficult to observe. The typical seismogenic depth is between 5 and 15 km
291 while deeper (~ 40 km) seismicity was detected only SW of Capo Calavà (see sections in the right
292 panel of Fig. 8A).

293 In order to obtain information on seismic faulting, fault plane solutions of earthquakes with $M > 2.7$
294 were selected from the RCMT and the “Sicily and Calabria focal mechanism database”
295 (<http://www.bo.ingv.it/RCMT>; <http://sismoweb.ct.ingv.it/focal/>; see Pondrelli et al., 2006; Scarfi et
296 al., 2013). As a whole, focal solutions suggest that seismogenic faulting occurs both on NW-SE and
297 on NE-SW trends according with two preferential and contrasting mechanisms (Fig. 8B). The NW-
298 SE nodal planes characterize events with dextral strike-slip or oblique movements mainly located
299 SW and S of the Vulcano Island. Instead, normal mechanism on NE-SW and NNE-SSW oriented
300 dislocation planes are dominant in the near-offshore and mainland roughly between Capo Milazzo
301 and Capo Tindari. A GIS-derived earthquake density map (Fig. 8C) estimated from the considered
302 time interval (1984–2014) was built up by using Kernel density algorithm (Silverman, 1986). The
303 map displays that the highest concentration of events takes place mainly in the mainland within the
304 Tindari-Barcellona tectonic depression (see section 3) and west of Capo Milazzo roughly along the
305 Patti ridge (see Fig. 3A for location).

306

307 **6. Kinematic reconstruction**

308 The integration of onshore and offshore datasets provides new insights into the structural
309 pattern and fault kinematic in an area of north-east Sicily and its offshore prolongation
310 characterized by frequent seismicity. Field analysis revealed that tectonic deformation is mainly
311 expressed by a major transtensional NW-SE trending tectonic boundary, the Tindari-Rocca Novara
312 fault zone, and subordinately by an array of NNE-SSW striking minor extensional faults, in
313 agreement with previous studies (e.g. Billi et al., 2006; De Guidi et al 2013). A first relevant
314 observation is that the Tindari-Rocca Novara fault segment could not be followed in the offshore as
315 expected, since it appears to terminate just off the coastline (see also Argnani et al., 2007). At the
316 same time, another major NW-SE trending fault zone has been found to the east, between the SE
317 flank of the Vulcano island and Capo Milazzo. This fault zone, here indicated as “Vulcano-Milazzo
318 fault zone”, is composed by a swarm of transtensional fault segments which appear to control the
319 main morpho-bathymetric features, i.e. the Patti Ridge and the Milazzo canyon (Fig. 6). West of

320 this tectonic alignment, an array of NNE-SSW oriented minor extensional faults occur, very similar
321 in trend and kinematics to those observed on-land. The general pattern of these minor extensional
322 faults, obtained by merging offshore and on-land data, depicts a lozenge-shaped tectonic depression
323 between two major bounding fault systems, the Tindari-Rocca Novara fault zone on-land and the
324 Vulcano-Milazzo fault zone offshore. Taking into account the right-lateral offset of the Tindari-
325 Rocca Novara Fault (see section 3 and Fig. 2 C) and inferring a similar movement for the Vulcano-
326 Milazzo Fault, based on the focal mechanism of the 1978 earthquake, the Gulf of Patti can be
327 tectonically interpreted as a dilatational stepover area developed between two major right-stepping,
328 right-lateral bounding fault systems (Fig. 9).

329 Even though a straightforward correlation between shallow faulting and the recorded
330 seismicity (mainly from 5 to 15 km depth, see Fig. 8A) cannot be directly inferred because of the
331 relatively low penetration of our seismic dataset, the indications provided by the focal plane
332 solutions (see section 5), within their intrinsic uncertainty, appear to support this interpretation. The
333 high-rate earthquake density also supports the proposed kinematic reconstruction since relay zones
334 are commonly regarded as sites of earthquake rupture nucleation (foreshock and/or aftershock
335 events, see also [Barka and Kadinsky-Cade, 1988](#); [Kadinsky-Cade and Barka, 1989](#)).

336

337 **7. Discussion and Conclusions**

338 An integrated analysis of field, seismological and marine geophysical data in the Gulf of
339 Patti (Tyrrhenian side of NE Sicily) allowed to provide new constraints on active faulting and on
340 the submarine morphological setting of this hazardous area. Particularly, the correlation between
341 field data with the offshore seismic investigation and morpho-bathymetry allowed to better
342 understand the structural pattern and fault kinematics of this sector of the NE-Sicily continental
343 margin. The major structural discontinuities recognized in the area consist of two right-lateral, NW-
344 SE trending transtensional fault zones, namely the Tindari-Rocca Novara, on-land, and the
345 Vulcano-Milazzo, offshore. In addition, NNE-SSW to and N-S striking extensional faults occur
346 mainly along the sector where the two larger fault zones overlap. Accordingly, the central portion of
347 the Gulf of Patti and its southward prolongation (i.e. the Tindari-Barcellona tectonic depression, see
348 [Billi et al., 2006](#)) is interpreted as releasing stepover (Fig. 9) resulting from a local stress
349 perturbation between two right-stepping, right lateral en-echelon arranged fault systems. We
350 exclude a releasing bend configuration since continuity between master faults have not been clearly
351 observed in the seismic profiles. Current and historical seismicity suggests that moderate
352 earthquakes ($1 < M < 4.6$) mainly occur within the releasing zone whereas major events (e.g. the 1786,

353 Mw=6.2; 1978, Mw=6.1, [Rovida et al., 2011](#)) are roughly aligned with the larger bounding faults
354 (see also [Barka and Kadinsky-Cade, 1988](#); [Kadinsky-Cade and Barka, 1989](#)).

355 Although it was not possible to identify first order crustal faults in the Gulf of Patti due to
356 the shallow penetration of our geophysical dataset, and hence the possible sources of the largest
357 earthquakes of the area went undetected, most of the faults mapped offshore show evidence of
358 active deformation as they offset Holocene deposits and locally also deform the seafloor. These
359 faults may be hence interpreted as secondary shallow structures linked to the deep, unidentified
360 seismogenic faults. The interpretation of morpho-bathymetric data has shown that the Gulf of Patti
361 offshore is characterized by a complex system of deeply-incised canyons and channels, extending
362 from the shelf margins down to deeper sectors. The over-steepening caused by the uplift of the
363 Capo Milazzo area induce both the emplacement of canyons and a diffuse slope instability in the
364 Gulf of Patti. The spatial distribution of both shallow and deep-seated slides reveals that slope
365 instability is mainly concentrated along the steep, fault-controlled, flanks of the major incisions,
366 thus allowing to hypothesize that the canyons should be still active morphological features. The
367 result of retrogressive erosional processes at the canyon head, which is documented by the intense
368 headward erosion, suggests a possible progressive approach and a potential erosional risk for the
369 present-day coastline (e.g. Colantoni branch), that may induce severe damage to the buildings and
370 artifacts in the next future.

371 In conclusion, our data indicate that the Gulf of Patti is a highly-critical region of the south-
372 eastern Tyrrhenian Sea, since it is currently affected by intense seismicity and submarine gravity
373 flows. Taking into account that the area hosts several villages as well as relevant infrastructures
374 (industrial sites, submarine gas pipelines, electric power and telecommunications cables) it
375 represents a vulnerable district in terms of geo-hazard.

376 **Appendix**

377 A grid of very high-resolution seismic reflection profiles was recorded along the continental
378 shelf and the slope of the Gulf of Patti, on board the R/V *Urania*, during January 2014. The lines run
379 mainly in the NE-SW direction and are tied by lines acquired in NW-SE direction (see Fig. A1 for
380 location). The acoustic source used during seismic prospecting was a 1 kJ Sparker power supply
381 with a multi-tips Sparker array, which avoids ringing and has a base frequency of about 800 Hz,
382 fired at a time interval of 2 s. Data was recorded using a single-channel streamer with an active
383 section of 2.8 m, containing seven high-resolution hydrophones, for 1.5 s two way time (t.w.t.) at a
384 10 kHz (0.1 ms) sampling rate. Positioning was ensured by a Differential Global Positioning
385 System (DGPS).

386 Data processing include: spherical divergence correction, de-ghosting, band-pass (300-2000
387 Hz) filter, swell filter, trace mixing, time variant gain, and mute of water column. Signal penetration
388 was found to exceed 500 ms t.w.t. The vertical resolution is ~1 m near the seafloor.

389 A set of ultra-high resolution reflection seismic data was also recorded by using the Chirp II
390 (Benthos©inc) Chirp sub-bottom profiler, operating with 16 transducer in a wide frequency band
391 (2–7 kHz) with a long pulse (20–30 ms). The lines have been acquired along the same directions of
392 the very high-resolution seismic reflection profiles.

393 Data processing include: a) true amplitude recovery using a T^2 spherical divergence
394 correction; b) time variant gain to boost amplitudes of deeper arrivals and c) mutes to eliminate the
395 signal noise on the water column. Signal penetration was found to exceed 90 ms two-way time
396 (t.w.t.). Vertical resolution is up to 5 cm near the seafloor.

397 All seismic lines were depth-converted. An average value of 1515 m/s for the sound velocity
398 was derived by the sound velocity profiles recorded during the multibeam data acquisition. Since
399 information was available on velocities of seismic units, we have adopted an average value of 1750
400 m/s for the sedimentary deposits. The adopted seismic velocities were based on sonic log data for
401 coeval sedimentary units drilled offshore Southern and Western Sicily (Pepe et al., 2010). However,
402 the inherent uncertainty of our approach does not influence the general frame of the structural
403 interpretation presented in this study.

404 **Acknowledgments**

405 The authors would like to thank the scientific team attending to the “Milazzo 2013” Cruise and the
406 crew of R/V Urania of the National Council of Researches (CNR) for their helpful support during
407 the geophysical survey. The guest editor Sebastiano D’Amico and two anonymous reviewers are
408 gratefully thanked for the accurate and constructive reviews of the manuscript. We thank Danilo
409 Morelli for the useful discussions about the structural setting of the Gulf of Patti. We dedicated two
410 canyon branches of the Milazzo Canyon to Paolo Colantoni and Francesco Fanucci, for their
411 precious contribute to the Italian marine geology. This work was partially funded by PRIN 2010-11
412 Project “Active and recent geodynamics of Calabrian Arc and accretionary complex in the Ionian
413 Sea” (responsible C. Monaco).

414 **References**

- 415 Argnani, A., E. Serpelloni, and C. Bonazzi (2007), Pattern of deformation around the central
416 Aeolian Islands: Evidence from multichannel seismics and GPS data, *Terra Nova*, 19, 317–323,
417 doi:10.1111/j.1365-3121.2007.00753.x.
- 418 Azzaro R., D'Amico S., Mostaccio A., Scarfi L., (2002). Terremoti con effetti macrosismici in
419 Sicilia orientale nel periodo Gennaio 1999 - Dicembre 2001. *QUADERNI DI GEOFISICA*, 27.

420 Azzaro R., D'Amico S., Mostaccio A., Scarfi L., Tuve' T., Manni M., (2014). Terremoti con effetti
421 macrosismici in Sicilia orientale nel periodo Gennaio 2009 - Dicembre 2013. QUADERNI DI
422 GEOFISICA, 120.

423 Barbano M.S., Bottari A., Carveni P., Cosentino M., Federico B., Fonte G., Lo Giudice E.,
424 Lombardo G. e Patané G. (1979). Macro seismic study of the gulf of Patti earthquake in the
425 geosstructural frame of North-Eastern Sicily. Bollettino della Società Geologica Italiana, vol. 98,
426 pp.155-174.

427 Barka, A. A. and Kadinsky-Cade, K. (1988). Strike-slip fault geometry in Turkey and its influence
428 on earthquake activity. *Tectonics*. 7, 663-684.

429 Barreca, G., V. Bruno, F. Cultrera, M. Mattia, C. Monaco and L. Scarfi (2014). New insights in the
430 geodynamics of the Lipari-Vulcano area (Aeolian Archipelago, southern Italy) from geological,
431 geodetic and seismological data, *Journal of Geodynamics*, 82, 150-167;
432 <http://dx.doi.org/10.1016/j.jog.2014.07.003>.

433 Barreca, G., L. Scarfi, F. Cannavò, I. Koulakov and C. Monaco (2016). New structural and
434 seismological evidence and interpretation of a lithospheric-scale shear zone at the southern edge
435 of the Ionian subduction system (central-eastern Sicily, Italy). *Tectonics*, 35,
436 doi:10.1002/2015TC004057.

437 Billi A., Barberi G., Faccenna C., Neri G., Pepe F. & Sulli F. (2006) - Tectonics and seismicity of
438 the Tindari Fault System, southern Italy: Crustal deformations at the transition between ongoing
439 contractional and extensional domains located above the edge of a subducting slab. *Tectonics*,
440 25, TC2006, doi:10.1029/2004TC001763.

441 Chiarabba C., De Gori P., Speranza F. (2008) - The southern Tyrrhenian subduction zone. Deep
442 geometry, magmatism and Plio-Pleistocene evolution. *Earth Planet. Sci. Lett.*, 268, 408-423,
443 doi:10.1016/j.epsl.2008.01.036.

444 Chiarabba, C., Jovane, L., Di Stefano, R., (2005). A new view of Italian seismicity using 20 years
445 of instrumental recordings. *Tectonophysics* 395 (34), 251–268.

446 Chiocci, F.L., Ercilla, G., Torres, J., (1997). Stratal architecture of western Mediterranean margins
447 as the result of the stacking of Quaternary lowstand deposits below 'glacio-eustatic fluctuation
448 base-level'. *Sedimentary Geology* 112, 195-217.

449 Colantoni P., Cuppari A., Gabbianelli G., Morelli D., (2001). The Milazzo Canyon and its mid-slop
450 depositional wedge on the Northern Sicilian Continental margin (Tyrrhenian Sea). *GeoActa*, v.
451 2001-2002, pp 15-26. Bologna.

- 452 Cuppari, A., Colantoni, P., Gabbianelli, G., Morelli, D., Alparone, R., (1999). Assetto ed
453 evoluzione morfo-strutturale dell'area marina compresa tra il margine della Sicilia settentrionale
454 e le Isole Eolie (Golfo di Patti). *Atti AIOL XIII*,137–149.
- 455 De Guidi G., Lanzafame G., Palano M., Puglisi G., Scaltrito A., Scarfi L. (2013) - Multidisciplinary
456 study of the Tindari Fault (Sicily, Italy) separating ongoing contractional and extensional
457 compartments along the active Africa–Eurasia convergent boundary. *Tectonophysics*, in print.
- 458 Di Stefano, A., and R. Lentini (1995), Ricostruzione stratigrafica e significato paleotettonico dei
459 depositi plio-pleistocenici del margine tirrenico tra Villafranca Tirrena e Faro (Sicilia nord-
460 orientale), *Studi Geol. Camerti*, 1995(2), 219 – 237.
- 461 Doglioni C., Innocenti F. & Mariotti G. (2001) - Why Mt Etna? *Terra Nova*, 13: 25-31.
- 462 Faccenna, C., Becker T.W., Lucente F.P., Jolivet L., Rossetti F. (2001) - History of subduction and
463 back-arc extension in the central Mediterranean. *Geophys. J. Int.*, 145, 809–820,
464 doi:10.1046/j.0956-540x.2001.01435.x.
- 465 Faccenna C., Piromallo C., Crespo-Blanc A., Jolivet L., Rossetti F. (2004) - Lateral slab
466 deformation and the origin of western Mediterranean arcs. *Tectonics*, 23, TC1012, doi:
467 10.1029/2002TC001488.
- 468 Ferranti, L., and J. S. Oldow (2005), Latest Miocene to Quaternary horizontal and vertical
469 displacement rates during simultaneous contraction and extension in the Southern Apennines
470 orogen, Italy, *Terra Nova*, 17, 209–214.
- 471 Ferranti L., Antonioli F., Mauz B., Amorosi A., Dai Pra G., Mastronuzzi G., Monaco C., Orru' P.,
472 Pappalardo M., Radtke U., Renda P., Romano P., Sanso' P., & Verrubbi V. (2006) - The last
473 glacial sea-level high stand along the coast of Italy. Tectonic implication. Contribution from the
474 32nd IGC, Editorial *Quat. Internat.*145-146, 30-54.
- 475 Frepoli A., Selvaggi G., Chiarabba C., Amato A. (1996) - State of stress in the Southern Tyrrhenian
476 Subduction Zone from fault-plane solutions. *Geophys. J. Int.*, 125, 879-891, doi: 10.1111/j.1365-
477 246X.1996.tb06031.x.
- 478 Gabbianelli G., Tramontana M, Colantoni P. Fanucci F., (1996) - Lineamenti morfostrutturali e
479 sismostratigrafici del Golfo di Patti (margine nord siciliano). In: F.M. Faranda & P. Povero
480 (Eds.): "Data Report". *Eocumm95*, Conisma, pp. 443-453.
- 481 Gallais, F., Graindorge, D., Gutscher, M.A., Klaeschen, D., (2013). Propagation of a lithospheric tear
482 fault (STEP) through the western boundary of the Calabrian accretionary wedge offshore eastern
483 Sicily (Southern Italy). *Tectonophysics* 602, 141–152.
484 <http://dx.doi.org/10.1016/j.tecto.2012.12.026>.

485 Gasparini, C., Iannaccone, G., Scandone, P., Scarpa, R., (1982). Seismotectonics of the Calabrian
486 Arc. *Tectonophysics* 82, 267–286.

487 Gasparini, C., Iannaccone, G., Scarpa, R., (1985). Fault-plane solutions and seismicity of the Italian
488 peninsula. *Tectonophysics* 117, 59–78.

489 Ghisetti F. (1979) - Evoluzione neotettonica dei principali sistemi di faglie della Calabria centrale.
490 *Bollettino Società Geologica Italiana*, 98, 387-430.

491 Giammanco, S., Palano, M., Scaltrito, A., Scarfi, L., Sortino, F., (2008). Possible role of fluid
492 overpressure in the generation of earthquake swarms in active tectonic areas: the case of the
493 Peloritani Mts. (Sicily, Italy). *Journal of Volcanology and Geothermal Research* 178, 795–806.
494 <http://dx.doi.org/10.1016/j.jvolgeores.2008.09.005>.

495 Goes S., Giardini D. Jenny S., Hollenstein C., Kahle H.G. & Geiger, A. (2004) - A recent tectonic
496 reorganization in the south-central Mediterranean. *Earth Planet. Sci. Lett.*, 226, 335-345.

497 Govers, R., Wortel, M.J.R., (2005). Lithosphere tearing at STEP faults: response to edges of
498 subduction zones. *Earth Planet. Sci. Lett.* 236, 505–523.

499 Guegen, E., Doglioni, C., Fernandez, M., (1998). On the post 25 Ma geodynamic evolution of the
500 western Mediterranean. *Tectonophysics* 298, 259–269.

501 Gutscher, M.-A., S. Dominguez, B. Mercier de Lepinay, L. Pinheiro, N. Babonneau, A. Cattaneo,
502 Y. Le Faou, G. Barreca, A. Micallef, and M. Rovere (2015), Tectonic expression of an active
503 slab-tear from high-resolution seismic and bathymetric data offshore Sicily (Ionian Sea),
504 *Tectonics*, 34, 39–54, doi:10.1002/2015TC003898.

505 Gvirtzman, Z., Nur, A., (1999). Formation of Mount Etna as a consequence of slabrollback. *Nature*
506 401, 782–785.

507 Kadinsky-Cade, K., and A. Aykut Barka, (1989). Effects of restraining bends on the rupture of
508 strike-slip earthquakes, U.S. Geol. Surv. Open-File Rep. 89-315, 181-192.

509 Kuhlmann, J., Asioli, A., Trincardi, F., Klügel, A., Huhn, K., (2015). Sedimentary response to
510 Milankovitch-type climatic oscillations and formation of sediment undulations: evidence from a
511 shallow-shelf setting at Gela Basin on the Sicilian continental margin. *Quaternary Science*
512 *Reviews* 108, 76-94

513 Lanzafame G. & Bousquet J.C. (1997) - The Maltese escarpment and its extension from Mt. Etna to
514 the Aeolian Islands (Sicily): importance and evolution of a lithosphere discontinuity. *Acta*
515 *Vulcanologica*, 9: 113-120.

516 Locardi, E., Nappi, G., (1979). Tettonica e vulcanismo recente nell'isola di Lipari (implicazioni
517 geodinamiche). *Boll. Soc. Geol. It.* 98, 447–456

518 Malinverno, A., Ryan W. B. F., (1986). Extension in the Tyrrhenian Sea and shortening in the
519 Apennines as result of arc migration driven by sinking of the lithosphere, *Tectonics*, 5(2), 227–
520 245, doi:10.1029/TC005i002p00227.

521 Neri, G., A. M. Marotta, B. Orecchio, D. Presti, C. Totaro, R. Barzaghi, Borghi A. (2012), How
522 lithospheric subduction changes along the Calabrian Arc in southern Italy: Geophysical
523 evidences, *Int. J. Earth Sci.*, doi:10.1007/s00531-012-0762-7.

524 Neri, G., Barberi, G., Oliva, G., Orecchio, B., (2004). Tectonic stress and seismogenic faulting in
525 the area of the 1908 Messina earthquake, south Italy. *Geophys. Res. Lett.* 31, 10 (doi:
526 10.1029/2004GL019742).

527 Nicolich R., Laigle M., Hirn A., Cernobori L., & Gallart J. (2000) - Crustal structure of the Ionian
528 margin of Sicily: Etna volcano in the frame of regional evolution. *Tectonophysics*, 329, 121 –
529 139.

530 Ogniben L. (1969) - Schema introduttivo alla geologia del Confine calabro-lucano. *Mem. Soc.*
531 *Geol. It.*, 8: 453-763.

532 Palano M., Ferranti L., Monaco C., Mattia M., Aloisi M., Bruno V., Cannavò F., Siligato G. (2012)
533 – GPS velocity and strain fields in Sicily and southern Calabria, Italy: Updated geodetic
534 constraints on tectonic block interaction in the central Mediterranean. *Journal of Geophysical*
535 *Research*, vol. 117, b07401, doi:10.1029/2012jb009254.

536 Patacca E., Sartori R., Scandone P. (1990) - Tyrrhenian basin and Apenninic arcs: Kinematic
537 relations since late Tortonian times. *Mem. Soc. Geol. Ital.*, 45, 425-451.

538 Pepe, F., G. Bertotti, F. Cella, and E. Marsella (2000), Rifted margin formation in the south
539 Tyrrhenian Sea: High resolution seismic profile across the north Sicily passive continental
540 margin, *Tectonics*, 19, 241 – 257.

541 Pepe, F., A. Sulli, M. Agate, D. Di Maio, A. Kok, C. Lo Iacono, and R. Catalano (2003). Plio-
542 Pleistocene geological evolution of the northern Sicily continental margin (southern Tyrrhenian
543 Sea): New insights from high-resolution, multi-electrode sparker profiles, *Geo Mar. Lett.*, 23 (1),
544 53–63.

545 Pepe, F., A. Sulli, G. Bertotti, and R. Catalano (2005), Structural highs formation and their
546 relationship to sedimentary basins in the north Sicily continental margin (southern Tyrrhenian
547 Sea): Implication for the Drepano Thrust Front, *Tectonophysics*, 409, 1–18.

548 Pepe, F., Bertotti, G., Ferranti, L., Sacchi, M., Collura, A.M., Passaro, S., Sulli, A., (2014). Pattern
549 and rate of post-20 ka vertical tectonic motion around the Capo Vaticano Promontory (W
550 Calabria, Italy) based on offshore geomorphological indicators, *Quat. Int.*, 30 (1), e14.

551 Polonia A., Torelli L., Artoni A., Carlini M., Faccenna C., Ferranti L., Gasperini L., Govers R.,
552 Klaeschen D., Monaco C., Neri G., Nijholt N., Orecchio B., Wortel R. M. (2016) – The Ionian
553 and Alfeo-Etna fault zones: New segments of an evolving plate boundary in the central
554 Mediterranean Sea? *Tectonophysics*, Doi: 10.1016/j.tecto.2016.03.016.

555 Pondrelli, S., S. Salimbeni, G. Ekström, A. Morelli, P. Gasperini, and G. Vannucci (2006), The
556 Italian CMT dataset from 1977 to the present, *Phys. Earth Planet. Inter.*,
557 <http://dx.doi.org/10.1016/j.pepi.2006.07.008>, 159/3-4, 286–303.

558 Ridente, D., Trincardi, F., (2002). Eustatic and tectonic control on deposition and lateral variability
559 of Quaternary regressive sequences in the Adriatic basin. *Mar. Geol.* 184 (3e4), 273-293.

560 Rosenbaum, G., Lister, G.S., (2004). Neogene and Quaternary rollback evolution of the Tyrrhenian
561 Sea, the Apennines, and the Sicilian Maghrebides. *Tectonics* 23, TC1013.
562 doi:10.1029/2003TC001518.

563 Rovere M., Gamberi F., Mercorella A., Leidi E., (2014). Geomorphometry of a submarine mass-
564 transport complex and relationships with active faults in a rapidly uplifting margin (Gioia Basin,
565 NE Sicily margin). *Marine Geology*, 356, 31–43.

566 Rovida, A., Camassi, R., Gasperini, P., Stucchi, M., (2011): CPTI11, the 2011 version of the
567 Parametric Catalogue of Italian Earthquakes. INGV, Milano, Bologna,
568 <http://emidius.mi.ingv.it/CPTI>, DOI:10.6092/INGV.IT-CPTI11.

569 Scarascia, S., A. Lozej, and R. Cassinis (1994), Crustal structures of the Ligurian, Tyrrhenian and
570 Ionian Sea and adjacent onshore areas interpreted from wide-angle seismic profile, *Boll. Geofis.*
571 *Teor. Appl.*, 36, 5 – 19.

572 Scarfì L., Barberi G., Musumeci C., Patanè D., (2014). Crustal structure and fault kinematics
573 between the Aeolian Arc and the Ionian Sea offshore as revealed by earthquake tomography and
574 focal mechanisms stress inversion, *Rendiconti Online della Società Geologica Italiana*, 31, doi:
575 10.3301/ROL.2014.140.

576 Scarfì, L., A. Messina, and C. Cassisi (2013), Sicily and Southern Calabria focal mechanism
577 database: a valuable tool for the local and regional stress field determination, *Ann. Geophys.*, 56,
578 1, D0109, doi:10.4401/ag-6109.

579 Scarfì, L., Langer, H., Scaltrito, A., (2005). Relocation of microearthquake swarms in the Peloritani
580 mountains—implications on the interpretation of seismotectonic patterns in NE Sicily, Italy.
581 *Geophysical Journal International* 163, 225–237. [http://dx.doi.org/10.1111/j.1365-](http://dx.doi.org/10.1111/j.1365-246X.2005.02720.x)
582 [246X.2005.02720.x](http://dx.doi.org/10.1111/j.1365-246X.2005.02720.x).

583 Scicchitano G., Spampinato C., Ferranti L., Antonioli F., Monaco C., Capano M., Lubritto C.
584 (2011) – Uplifted Holocene shorelines at Capo Milazzo (NE Sicily, Italy): evidence of co-

585 seismic and steady-state deformation. *Quaternary International*, 232, 201-213, doi: 10.1016/j-
586 quaint.2010.06.028.

587 Selvaggi, G., and C. Chiarabba (1995), Seismicity and P-wave velocity image of the Southern
588 Tyrrhenian subduction zone, *Geophys. J. Int.*, 121, 818– 826.

589 Silverman, B.W., 1986. *Density Estimation for Statistics and Data Analysis*. Chapman and Hall,
590 New York.

591 Wortel M.J.R. & Spakman W. (2000) - Subduction and slab detachment in the Mediterranean-
592 Carpathian region. *Science*, 290, 1910-1917

593

594 **Figure captions**

595 Fig. 1 - A) Tectonic sketch map of the Calabrian Arc area and relative off-shore; the red rectangle
596 represents the investigated area (SFTB, Sicilian fold and thrust belt; HB, Hyblean block). B) Map
597 view of the earthquakes with a maximum hypocentral depth of 40 km occurred in the study area
598 from 1984 to 2014. C) Simplified structural map of the SE sector of the Tyrrhenian Basin (CPT,
599 Calabro-Peloritani terrane). The NNW–SSE striking Aeolian–Tindari–Letojanni Fault System
600 (ATLFS) represents an incipient transfer zone (Billi et al., 2006; Barreca et al., 2014) separating a
601 contractional domain, to the west, from an extensional one to the north-east (see inset in Fig 1 C).
602 Focal mechanism of April 15, 1978 earthquake ($M_w=6.1$, see Gasparini et al., 1982) is also
603 reported.

604 Fig. 2 - A) Structural map of the onshore sector of the Aeolian-Tindari-Letojanni Fault System and
605 most representative stereoplots (red, fault plane and slip vectors; dashed black lines indicate
606 fractures). The inset shows the cumulative plots of the detected faults (fault planes and slip vectors,
607 at the top) and fractures (rose diagram, at the bottom). B) NW-SE trending oblique (transtensional)
608 fault segment singled out along the Capo Tindari cliff. C) NW-SE trending striated fault plane with
609 slickenlines plunging at $\sim 60^\circ$ towards N130E. D) NNE-SSW trending extensional fault segment
610 detected within the Tindari-Barcellona tectonic depression where it displaces middle Pleistocene
611 deposits. This fault set is mainly composed by steeply-dipping structures with pure ($\sim 90^\circ$ pitch)
612 normal sense of motion (E).

613 Fig. 3 – A) Morpho-bathymetric map of the Gulf of Patti as derived by the analysis of a 20x20 m
614 resolution DTM (in the background). B) 3D view of a deep-seated gravitational deformation
615 affecting the Fanucci branch of the Milazzo canyon.

616 Fig. 4 – Sparker profile SP 13 (see inset for location) showing the most recent sequence which
617 overlays a widespread erosional surface that ostensibly formed during the sea level stillstand of the
618 Last Glacial Maximum (LGM). Vertical exaggeration = 4:1 (4X).

619 Fig. 5 – Interpretation of the depth converted single channel seismic profiles acquired in the Gulf of
620 Patti (see inset in the bottom right corner for location). A) Sparker profile SP 19 showing horst and
621 graben structures (B) locally involving Holocene deposits. Bounding faults sometimes produce
622 straight, 15-20 m high fault scarps. C) Chirp profile CHP 43 showing a NNW-SSE oriented
623 extensional (or transtensional) fault segment (D) dislocating Holocene deposits of about 3 m. E)

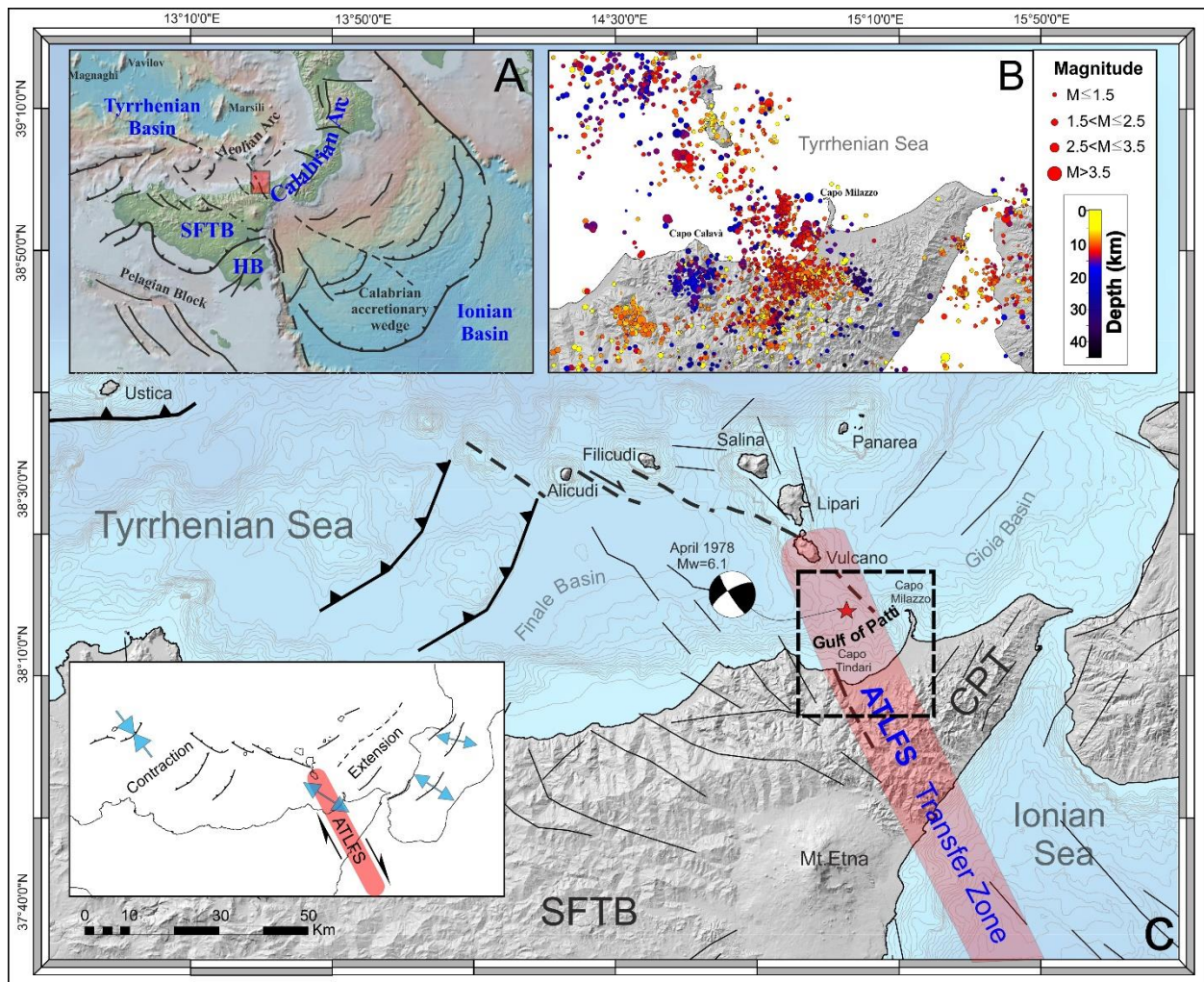


Figure 1

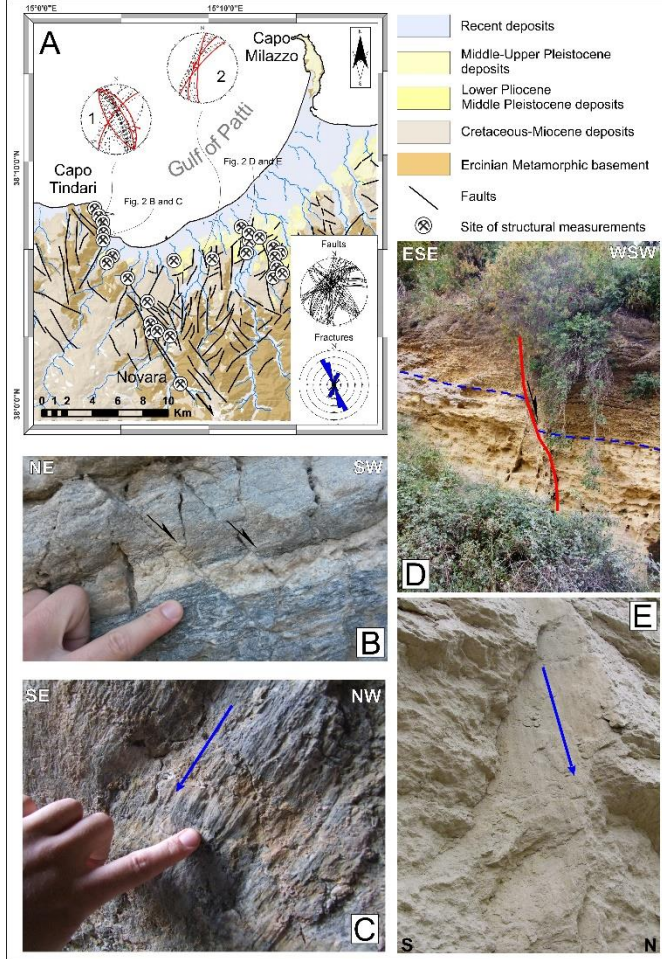


Figure 2

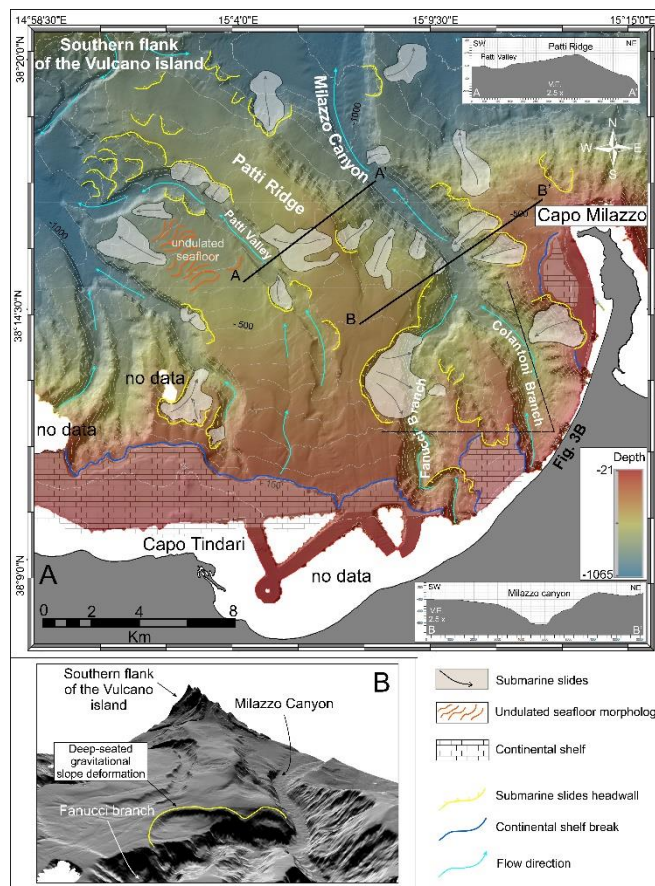


Figure 3

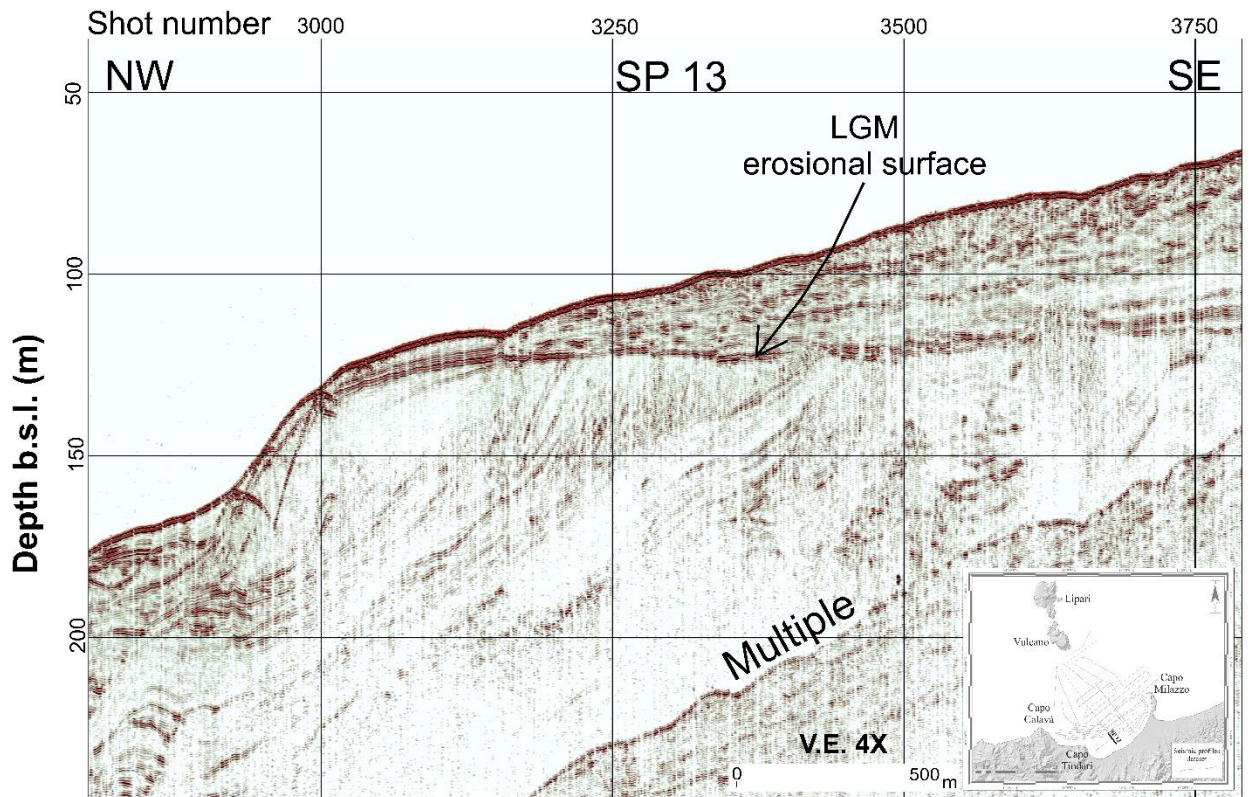


Figure 4

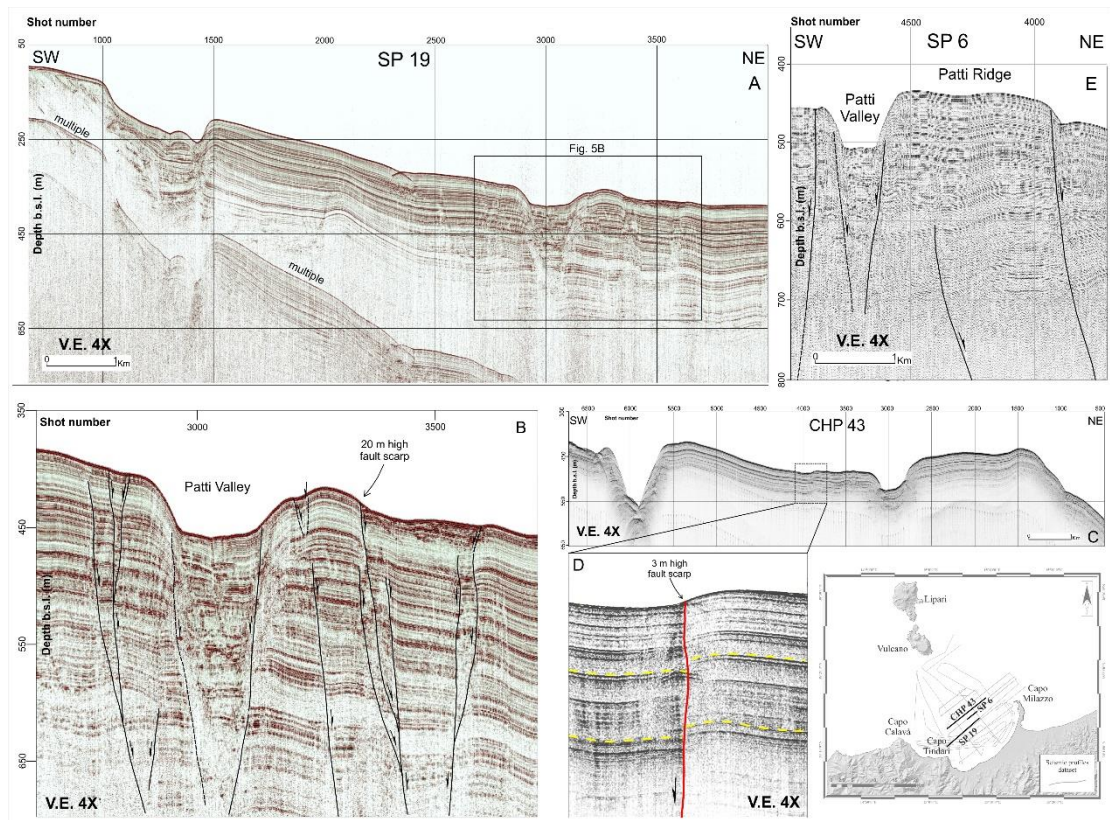


Figure 5

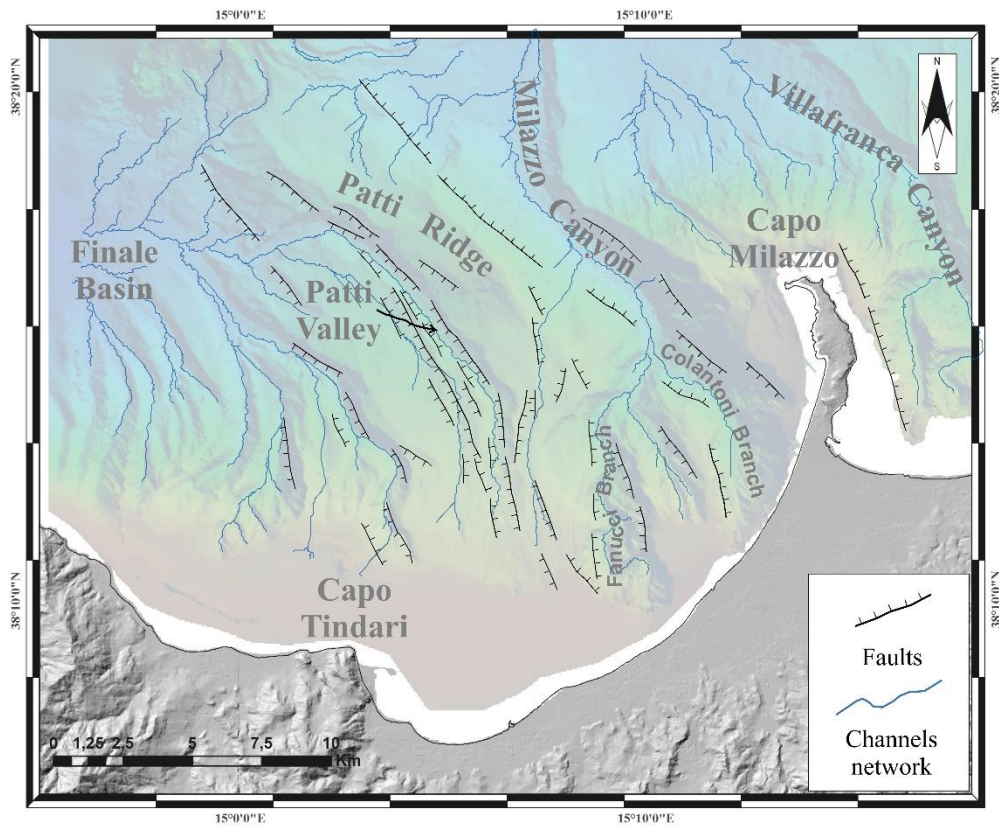


Figure 6

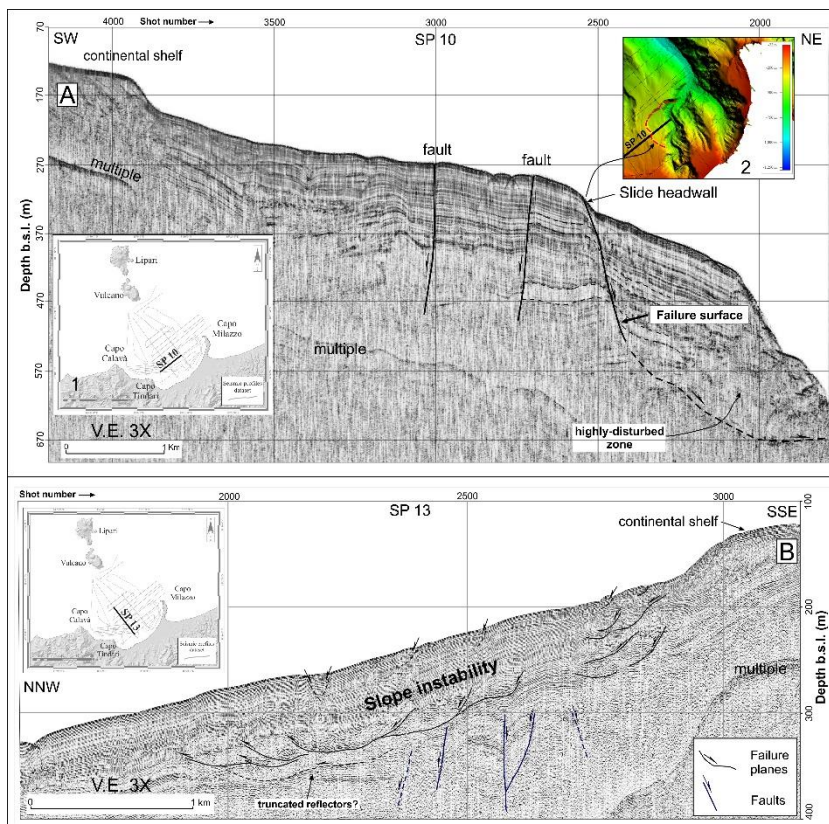


Figure 7

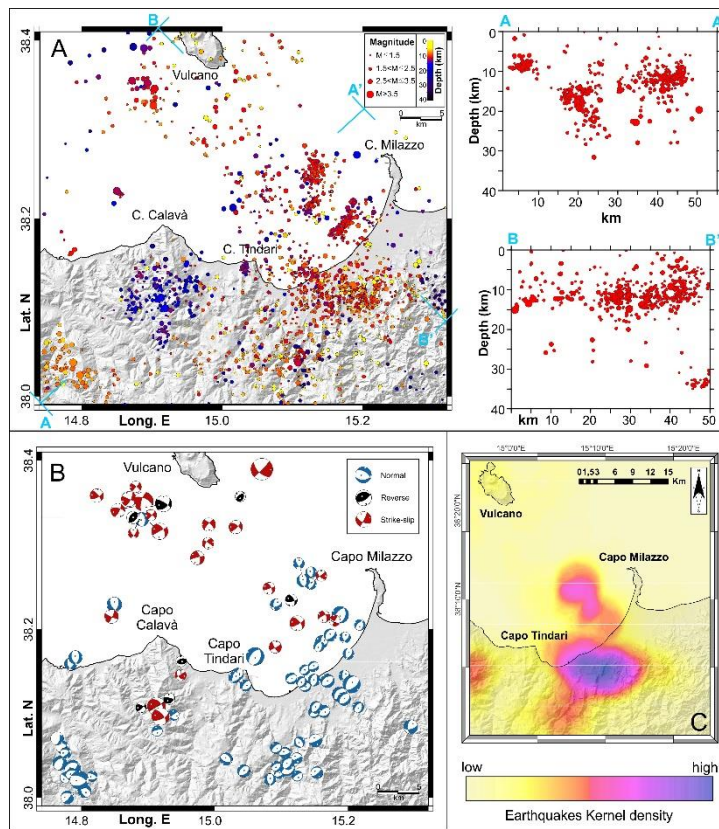


Figure 8

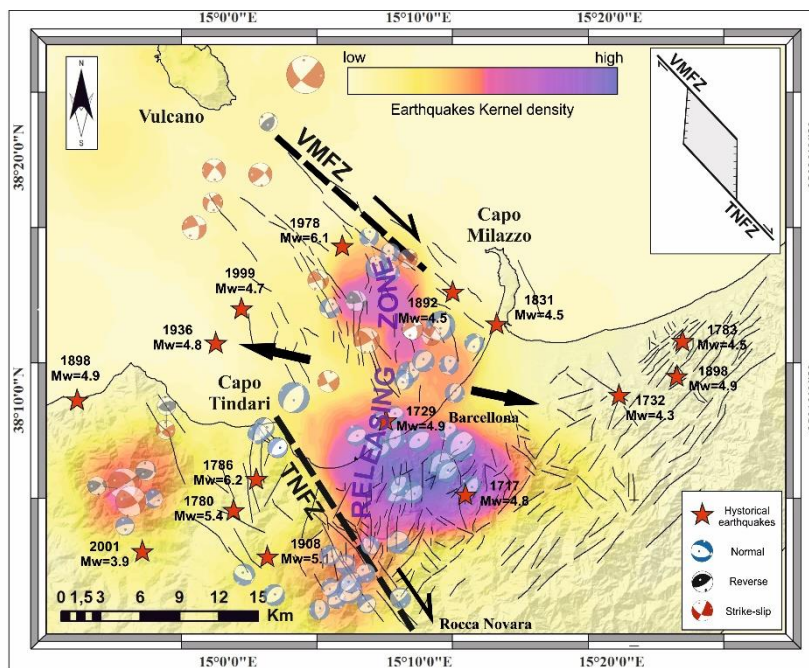


Figure 9

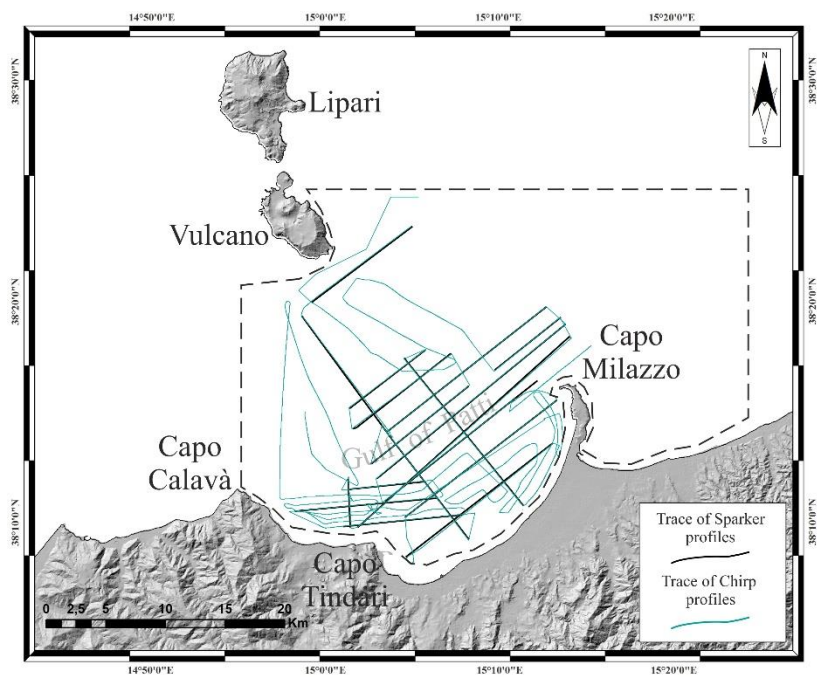


Figure A1

624 Sparker profile SP 6 showing the extensional (or transtensional) fault segments affecting the Patti
625 Ridge. Vertical exaggeration = 4:1 (4X).

626 Fig. 6 - Structural map of the Gulf of Patti obtained by picking fault segments on the whole seismic
627 dataset. Detected faults mainly consist of extensional (or transtensional) structures arranged into
628 two azimuthal (NW-SE and ~N-S trending) domains. Faults associated with a clear gravitational
629 deformation have not been reported in the structural map.

630 Fig. 7 - A) Sparker profile SP 10 (see inset 1 for location) showing two extensional (or
631 transtensional) fault segments, in the western part of the section, and a deep-seated gravitational
632 slope deformation in the eastern one (see shaded relief in inset 2 for slide headwall location). B)
633 Sparker profile SP13 (see inset for location) showing gravitational deformation (slumping) along
634 the continental slope. Vertical exaggeration = 3:1 (3X) for both profiles.

635 Fig. 8 - A) Earthquakes locations (1984-2014 period) in map and vertical sections. Cross-sections
636 (AA', BB') marked in map, incorporate all relocated events within 5 km of the cross-section lines.
637 B) Computed fault plane solutions (lower-hemisphere projection). C) Gis-derived earthquakes
638 density map estimated by using Kernel density algorithm (see text for further detail).

639 Fig. 9 – Kinematic reconstruction proposed for the Gulf of Patti and its onshore sector (earthquakes
640 density map in the background). The main NW-SE trending right-lateral transtensional fault zones
641 (TNFZ and VMFZ) overlap in right-stepping geometry likely forming a releasing zone in the relay
642 area, where minor ~ N-S oriented extensional faults occur. Note that most of seismicity occurring in
643 the investigated area appear confined within the releasing zone (see text for further detail). Location
644 of computed focal mechanisms and historical earthquakes (red stars, from [Rovida et al., 2011](#)) is
645 also reported.

646 Fig. A1. Grid of single-channel seismic profiles acquired in the Gulf of Patti. Green and black lines
647 indicate Chirp and Sparker profiles, respectively. Dashed rectangle indicates the area of multibeam
648 survey.